Three-body Hydrogen Bond Defects Contribute Significantly to the Dielectric Properties of the Liquid Water-Vapor Interface

Sucheol Shin and Adam P. Willard*

Department of Chemistry, Massachusetts Institute of Technology, Cambridge, Massachusetts 02139, USA

(Dated: October 11, 2017)

In this Letter, we evaluate the relationship between aqueous hydrogen bonding and interfacial molecular structure at the liquid water-vapor interface. We present a mean-field model of interfacial structure that can be used to compute the depth dependent orientational distribution of water molecules. Using this model we demonstrate that the primary features of water's interfacial molecular structure reflect the hydrogen bonding preferences of individual water molecules immersed within the anisotropic mean interfacial density field. We find that the polarization and polarizability of the interfacial environment are sensitive to distortions in the hydrogen bonding network that arise due to correlated molecular interactions. We identify a specific type of three-body hydrogen bond defect that is preferentially stabilized at the interface and contributes significantly to these interfacial properties. Our results reveal that the dielectric properties of the liquid water interfaces are influenced by collective molecular interactions that are unique to the interfacial environment.

The dielectric properties of liquid water are determined in large part by the orientational fluctuations of dipolar water molecules [1-4]. Near a liquid water-vapor interface these orientational fluctuations are anisotropic, leading to dielectric properties that differ significantly from their bulk values [5–7]. These differences are fundamental to interface-selective chemical and physical processes [8–11], but they are generally difficult to predict without the use of atomistic simulation [12, 13]. In this Letter, we attempt to understand these differences in terms of the statistical mechanics of hydrogen bonding at the liquid water-vapor interface. Using a mean-field model, we demonstrate that the primary features of water's interfacial molecular structure are determined by the molecular orientations that best facilitate tetrahedral hydrogen bonding within the constraints imposed by the anisotropic interfacial density field. Using this model, we show that interface-specific variations in the orientational polarization and polarizability are the results of distorted non-tetrahedral hydrogen bonding structures that arise due to correlated molecular interactions. By analyzing the results of atomistic simulation we identify a specific type of non-tetrahedral hydrogen bond defect that is preferentially stabilized at the interface by threebody interactions. We then show that defects of this type contribute significantly to the unique dielectric properties of the interfacial environment.

Our microscopic understanding of interfacial molecular structure derives primarily from a combination of surface-sensitive experiments, such as vibrational sum frequency generation [14–17], and atomistic simulation [18–21]. This combination has revealed that the interfacial environment contains depth dependent molecular populations that vary in their orientational alignments. The details of this depth-dependent orientational molecular structure cannot be completely determined from existing experimental data alone, so we currently rely on molecular simulation to make up for our lack of experi-

mental resolution. The structural predictions of molecular dynamics simulations carried out using classical force-fields are consistent with the available experimental data [22, 23]. Based on this consistency we treat the resulting interfacial structure as a reference to parameterize our model and evaluate its performance, noting that we would expect similar results if we based our model on more computationally expensive first-principles simulations [24].

Atomistic simulations of the liquid-vapor interface exhibit capillary wave-like undulations in the position of the liquid surface [25, 26]. These undulations are problematic for studies of interfacial molecular structure because they tend to blur out may of the molecular details. To avoid this, we utilize the dynamic frame of reference of the intrinsic interface [21]. In this frame of reference, molecular coordinates are defined relative to the time varying position of the instantaneous liquid phase boundary. This method effectively projects out the inherent spatial deformations of the liquid interface, leaving behind only the intrinsic molecular details. Since the deformations that are projected out in this reference frame are well characterized by capillary wave theory [27–30], their omitted effects are trivial to reincorporate. To transform into the reference frame of the intrinsic interface we follow the procedure described in Ref. 21.

Atomistic simulations have revealed that molecular structure of the intrinsic water-vapor interface is anisotropic extending about 1 nm into the bulk liquid [21, 31]. This anisotropic molecular structure can be decomposed into two separate components: (1) an interfacial density field, $\rho(\mathbf{r})$, where \mathbf{r} denotes the position measured relative to the instantaneous interface, and (2) a position-dependent probability distribution for molecular orientations, $P(\vec{\kappa}|\mathbf{r})$, where $\vec{\kappa}$ uniquely specifies the rotational configuration of a water molecule. The interplay between these two components is mediated by a combination of molecular packing effects and collec-

tive hydrogen bonding interactions. Here we consider only one side of this interplay by focusing specifically on $P(\vec{\kappa}|\mathbf{r})$ and how it is influenced by the characteristics of $\rho(\mathbf{r})$. We show that the general structure of $P(\vec{\kappa}|\mathbf{r})$ can be determined simply by considering the influence of $\rho(\mathbf{r})$ on the hydrogen bond preferences of a individual water molecules.

To formalize the relationship between $P(\vec{\kappa}|\mathbf{r})$ and $\rho(\mathbf{r})$ we have developed a mean-field model of interfacial hydrogen bonding. In our model, $P(\vec{\kappa}|\mathbf{r})$ is computed based on the orientational preferences of a single probe molecule immersed in the anisotropic mean density field of the intrinsic interface, $\rho(\mathbf{r})$. As illustrated in Fig. 1(a), the probe molecule is modeled as a point particle with four tetrahedrally coordinated hydrogen bond vectors, denoted \mathbf{b}_1 , \mathbf{b}_2 , \mathbf{b}_3 , and \mathbf{b}_4 . The length of these vectors are chosen to correspond to that of a hydrogen bond, so that each vector indicates the preferred position of a hydrogen bond partner. The absolute orientations of these tetrahedral hydrogen bond vectors are specified by $\vec{\kappa}$. Furthermore, to mimic the hydrogen bonding properties of water, each bond vector is assigned a directionality, with \mathbf{b}_1 and \mathbf{b}_2 acting as hydrogen bond donors and \mathbf{b}_3 and \mathbf{b}_4 acting as hydrogen bond acceptors.

The probe molecule interacts with the interfacial density field via an empirical hydrogen bonding potential. This potential specifies the energy of a probe molecule with position \mathbf{r} and orientation $\vec{\kappa}$ as,

$$E(\vec{\kappa}, \mathbf{r}) = \sum_{i=1}^{4} \epsilon_{\mathbf{w}} n_i(\mathbf{r}, \mathbf{b}_i) , \qquad (1)$$

where $\epsilon_{\mathbf{w}}$ is the energy associated with forming a hydrogen bond and n_i is a binary variable that indicates the hydrogen bonding state of the *i*th bond vector. Specifically, $n_i = 1$ if the probe molecule has formed a hydrogen bond along \mathbf{b}_i , and $n_i = 0$ if it has not. We treat the n_i 's as independent random variables that are distributed according to,

$$n_i(\mathbf{r}, \mathbf{b}_i) = \begin{cases} 1, & \text{with probability } P_{\text{HB}}(\mathbf{r}_i), \\ 0, & \text{with probability } 1 - P_{\text{HB}}(\mathbf{r}_i), \end{cases}$$
 (2)

where $\mathbf{r}_i = \mathbf{r} + \mathbf{b}_i$ denotes the terminal position of the *i*th bond vector and $P_{\text{HB}}(\mathbf{r}_i)$ specifies the probability for successful hydrogen bonding at position \mathbf{r}_i .

In the context of this model, the probability for a molecule at position \mathbf{r} to adopt a given orientation, $\vec{\kappa}$, can thus be expressed as,

$$P(\vec{\kappa}|\mathbf{r}) = \left\langle e^{-\beta E(\vec{\kappa},\mathbf{r})} \right\rangle_{\mathbf{h}} / Z(\mathbf{r}), \tag{3}$$

where $\langle \cdots \rangle_b$ denotes an average over all possible hydrogen bonding states (*i.e.*, variations in the n_i 's), $1/\beta$ is the Boltzmann constant, k_B , times temperature T, and $Z(\mathbf{r}) = \int d\vec{\kappa} \left\langle e^{-\beta E(\vec{\kappa},\mathbf{r})} \right\rangle_b$ is the orientational partition

function for the probe molecule at position **r**. By evaluating the average explicitly, the numerator of Eq. (3) can be written as,

$$\left\langle e^{-\beta E(\vec{\kappa}, \mathbf{r})} \right\rangle_{\mathbf{b}} = \prod_{i=1}^{4} \left[1 + P_{\mathbf{HB}} \left(\mathbf{r}_i \right) (e^{-\beta \epsilon_{\mathbf{w}}} - 1) \right].$$
 (4)

Together, Eqs. (3) and (4) provide a general analytical framework for computing the orientational molecular structure of an interface with a given density profile.

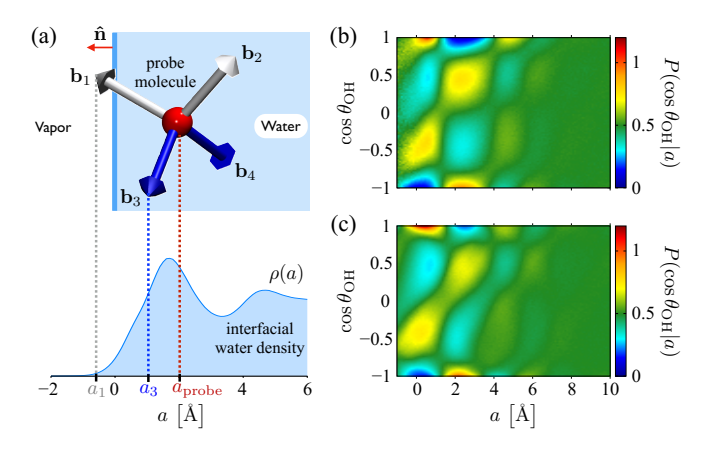


FIG. 1. (a) Schematic depiction of the mean-field model showing a probe molecule with tetrahedrally coordinated bond vectors (white for donor, blue for acceptor) within the liquid (blue shaded region) at a distance $a_{\rm probe}$ from the position of the instantaneous interface (solid blue line). A plot of the interfacial density profile, $\rho(a)$, obtained from the MD simulation with TIP5P water [32], is shown with dotted lines indicating the termination points of bond vectors \mathbf{b}_1 and \mathbf{b}_3 . Panels (b) and (c) contain plots of the orientational distribution function, $P(\cos\theta_{\rm OH}|a)$ (see Eq. (5)), as indicated by shading, computed from atomistic simulation and from the rigid tetrahedral model respectively.

In this model, molecular orientations are determined only through direct hydrogen bonding interactions. The properties of these interactions are specified by the geometry of the bond vectors, the hydrogen bond probabilities, $P_{\rm HB}(\mathbf{r})$, and the form of energy function in Eq. (1). Variations in hydrogen bonding geometry can be described by allowing the \mathbf{b}_i 's to vary in length and relative angle, and non-geometric variations in hydrogen bonding, such as orientational correlations, can be described by modifying the characteristics of $E(\vec{\kappa}, \mathbf{r})$ and $P_{\rm HB}(\mathbf{r}_i)$. The ability to vary the functional description of hydrogen bonding in this model enables a systematic approach to investigating the microscopic origins of interfacial molecular structure.

In this Letter, we simplify $P_{\rm HB}(\mathbf{r}_i)$ by assuming that the probability to form a hydrogen bond at position \mathbf{r}_i is simply proportional to the mean water density at that position, *i.e.*, $P_{\rm HB}(\mathbf{r}_i) \propto \rho(\mathbf{r}_i)$, where the value of the proportionality constant is based on bulk hydrogen bonding

statistics. Furthermore, we assume that the intrinsic interface is laterally isotropic and planar on length scales $\sim d_{\rm HB}$. This assumption enables the interfacial density field to be described in terms of an one-dimensional function, $\rho(a)$, where a denotes the distance from the instantaneous interface measured perpendicular to the interfacial plane, *i.e.*, the depth into the liquid. The function $P_{\rm HB}$ is similarly simplified by this assumption, taking the form $P_{\rm HB}(a_i) \propto \rho(a_i)$, where a_i is given by $a_i = a - \mathbf{b}_i \cdot \hat{\mathbf{n}}$, and $\hat{\mathbf{n}}$ is the unit vector normal to the plane of the interface (see Fig. 1(a)).

For the results presented below, we present comparisons of our model specifically to the results of classical simulations with the TIP5P force field [33], although we have compared to other standard force fields and found them to yield similar results and identical conclusions [32]. For statistical and graphical convenience we express this comparison in terms of the reduced orientational distribution function,

$$P(\cos \theta_{\rm OH}|a) = \int d\vec{\kappa} P(\vec{\kappa}|a) \left[\frac{1}{2} \sum_{i=1}^{2} \delta(\cos \theta_i - \cos \theta_{\rm OH}) \right],$$
(5)

where the summation is taken over the two donor bond vectors, $\cos \theta_i = \mathbf{b}_i \cdot \hat{\mathbf{n}}/|\mathbf{b}_i|$, and $\delta(x)$ is the Dirac delta function. We determine the one free parameter in our model, $\epsilon_{\rm w}$, by minimizing the Kullback-Leibler divergence between $P(\cos \theta_{\rm OH}|a)$ computed from our model and that from atomistic simulation [32]. This parameterization yields $\epsilon_{\rm w} = -1.4\,k_{\rm B}T$. Notably, this value is significantly lower than typical hydrogen bond energies [34, 35]. We reconcile this apparent discrepancy by noting that the model parameter $\epsilon_{\rm w}$ represents an effective hydrogen bond energy, and therefore includes the stabilizing effects of the liquid environment on broken or highly distorted hydrogen bonds that have been observed through X-ray absorption [36, 37].

The orientational polarization and polarizability of the liquid water-vapor interface can be computed from $P(\vec{\kappa}|a)$. We specify orientational polarization in terms of the average dipole field,

$$\langle \mu_{\hat{\mathbf{n}}}(a) \rangle = \mu_{\mathbf{w}} \int d\vec{\kappa} P(\vec{\kappa}|a) \left[\hat{\boldsymbol{\mu}}(\vec{\kappa}) \cdot \hat{\mathbf{n}} \right],$$
 (6)

where $\hat{\boldsymbol{\mu}}(\vec{\kappa})$ is the unit dipole vector of tagged molecule in particular orientation (i.e., $\hat{\boldsymbol{\mu}} = (\mathbf{b}_1 + \mathbf{b}_2)/|\mathbf{b}_1 + \mathbf{b}_2|$) and $\mu_{\rm w}$ is the dipole moment of an individual water molecule. Similarly, the orientational polarizability can be related to the fluctuations in the dipole field [2],

$$\langle (\delta \mu_{\hat{\mathbf{n}}}(a))^2 \rangle = \mu_{\mathbf{w}}^2 \int d\vec{\kappa} P(\vec{\kappa}|a) \left[\hat{\boldsymbol{\mu}}(\vec{\kappa}) \cdot \hat{\mathbf{n}} \right]^2 - \langle \mu_{\hat{\mathbf{n}}}(a) \rangle^2. \tag{7}$$

We evaluate the accuracy of our model by comparing the functions in Eqs. (5)-(7) to the same quantities computed from atomistic simulations.

We begin by considering an idealized implementation of our model in which the hydrogen bond vectors are of fixed length, $d_{\rm HB}=2.8\,\mbox{Å}$ (i.e., the equilibrium hydrogen bond distance [35]), and rigidly arranged with perfectly tetrahedral order. As illustrated in Fig. 1(b)-(c), this rigid tetrahedral model exhibits the same depth dependent patterns that have been observed in simulation results. The close qualitative agreement in $P(\cos\theta_{\rm OH}|a)$ between the rigid tetrahedral model and atomistic simulation implies that the orientational molecular structure of the liquid water-vapor interface is dominated by simple density-driven constraints on local hydrogen bonding.

Despite the ability of the rigid tetrahedral model to reproduce the structure of $P(\cos \theta_{\rm OH}|a)$ from atomistic simulation, it fails to accurately describe interfacial variations in orientational polarization and polarizability. We observe that atomistic simulation predicts significant changes in both $\langle \mu_{\hat{\mathbf{n}}}(a) \rangle$ and $\langle (\delta \mu_{\hat{\mathbf{n}}}(a))^2 \rangle$ at the interface, whereas these variations are not captured by the rigid tetrahedral model, which actually predicts no depth dependence in these quantities (Fig. 2). This depthindependent behavior is a mathematical consequence of the assumptions that hydrogen bonding is perfectly tetrahedral and energetically symmetric [38]. Interfacial variations in orientational polarization and polarizability must therefore arise through a combination of (1) distortions in tetrahedral coordination geometry and (2) asymmetry in donor/acceptor hydrogen bond energies. These effects can emerge spontaneously in the bulk liquid due to thermal fluctuations, however, they are highly exaggerated in the vicinity of the liquid-vapor interface as the result of correlated molecular interactions.

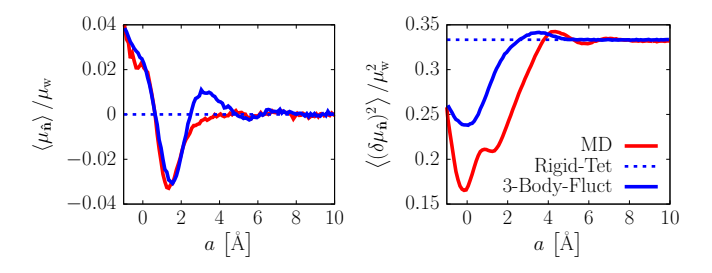


FIG. 2. Interfacial mean dipole orientation, $\langle \mu_{\hat{\mathbf{n}}}(a) \rangle$, and dipole fluctuations, $\langle (\delta \mu_{\hat{\mathbf{n}}}(a))^2 \rangle$, computed from atomistic simulation and our mean-field model with different implementations. Solid red lines (MD) correspond to atomistic simulation data. Dashed (Rigid-Tet) and solid (3-Body-Fluct) blue lines correspond to the rigid tetrahedral model and the three-body fluctuation model (see Eq. (8)), respectively.

We quantify the hydrogen bond geometry of individual molecules by specifying the *inter-bond* angle, ψ , between pairs of hydrogen bonds. As Fig. 3(a) illustrates, there are six such angles for a molecule with four unique hydrogen bond partners. The probability distribution for this angle, $P(\psi)$, computed from atomistic simulation is plotted in Fig. 3(b). This plot highlights that the interfacial

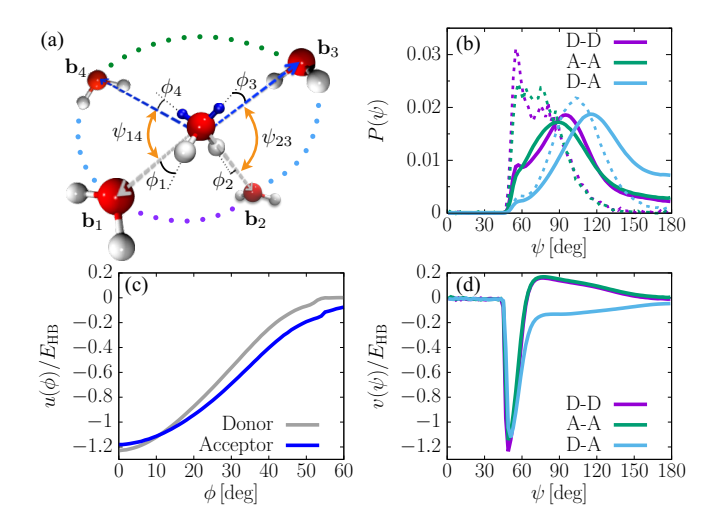


FIG. 3. (a) A schematic illustration of the angles used to quantify hydrogen bond geometries. (b) Probability distributions for inter-bond angles, ψ , generated from atomistic simulation, computed separately for donor-donor (D-D), acceptoracceptor (A-A), and donor-acceptor (D-A) pairs of bonds [32]. Solid and dashed lines correspond to statistics generated within the bulk liquid and at the interface (i.e., |a| < .1 Å) respectively. (c) Average direct interaction energy, $u(\phi)$, expressed in units of the average bulk hydrogen bond energy, $E_{\rm HB} = 9.0 \, k_B T$, between a tagged molecule and individual hydrogen bond partners, computed separately for donor and acceptor bonds. (d) Average direct interaction energy, $v(\psi)$, between two hydrogen bond partners of a tagged molecule, as indicated by the dotted arcs in panel (a), computed separately for the case of two donor partners, two acceptor partners, and one acceptor and one donor.

environment features highly distorted non-ideal hydrogen bond geometries that depend on the directionality (i.e., donor or acceptor) of the two adjacent hydrogen bonds. Specifically interfacial inter-bond angles are narrowed relative to that of the bulk, and this narrowing is especially significant between bonds with like directionality. Furthermore, as illustrated in Fig. 4(a), we observe a significant increase in the relative fraction of highly distorted hydrogen bond configurations within the first $2\,\text{Å}$ of the interfacial region.

The energetic properties of these highly distorted hydrogen bonds differ from those that are typical of the bulk liquid. For instance, as Fig. 3(c) illustrates, the average direct interaction energy between a tagged molecule and one of its hydrogen bond partners is significantly weakened when the bond is distorted away from its preferred tetrahedral geometry (i.e., ϕ is increased). Despite this weakening, however, we observe that highly non-ideal hydrogen bond configurations can be stabilized by favorable interactions between hydrogen bond partners. As Fig. 3(d) illustrates, these interactions become particularly favorable when $\psi \approx 60$ deg, where the hydrogen bond partners are separated by approximately $d_{\rm HB}$, and thus well situated to form a hydro-

gen bond. The resulting structure, a triangular threebody hydrogen bond defect, is ultimately unfavorable in the bulk liquid where many alternate configurations exist that satisfy the hydrogen bonding preferences of all three molecules without requiring significant geometric distortion. At the interface, however, this defect is stabilized by an increased availability of broken hydrogen bonds [39]. Due to the presence of the liquid phase boundary, these broken bonds cannot all be satisfied without significant distortions in hydrogen bond geometries. We quantify this stabilizing effect by computing the relative free energy for squeezed triangular hydrogen bond defects, $\beta \Delta F_{\text{sqz}}(a) = -\ln \left[P_{\text{sqz}}(a) / (1 - P_{\text{sqz}}(a)) \right], \text{ where } P_{\text{sqz}}(a)$ denotes the probability to observe a molecule with position a that is part of such a defect [32]. As Fig. 4(b)illustrates, these defects are more stable at the interface than in the bulk liquid by about $2k_BT$.

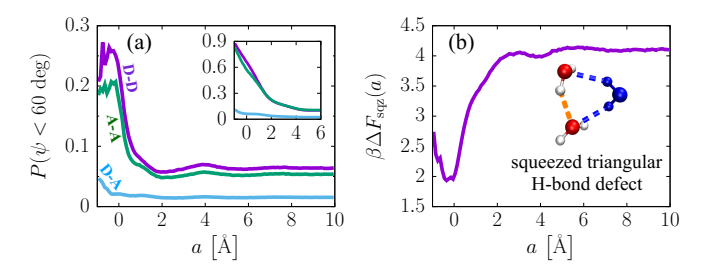


FIG. 4. (a) Probability of observing $\psi < 60$ deg at varied interfacial depth from the atomistic simulation and our model (inset). Labels indicating the types of bond pairs are given in the same colors of lines. (b) Interfacial profile of free energy change associated with the distortion into a squeezed triangular hydrogen bond defect. Plot shown above is for the case including two donor bonds.

The interfacial polarization and polarizability are significantly affected by the geometric distortions that arise due to interfacial hydrogen bond defects. The effects of these three-body interactions can be incorporated into our theoretical framework by modifying the rigid tetrahedral model to include an angle-dependent hydrogen bond energy, to mimic Fig. 3(c), and by including an empirical term to describe the energetic stabilization of triangular hydrogen bond defects. To do this we allow the relative angles of the bond vectors to fluctuate subject to the energetic variations observed in molecular simulation data. Specifically, in the three-body fluctuation model, we describe the energy of the probe molecule as,

$$E(\vec{\kappa}, a) = \sum_{i=1}^{4} \tilde{u}_{\alpha}(\phi_i) n_i + \sum_{i < j} \left[\tilde{v}_{\alpha\gamma}(\psi_{ij}) - \lambda_{\alpha\gamma}(a_i, a_j, \psi_{ij}) \right] n_i n_j,$$
(8)

where ϕ_i denotes the angle of deviation of \mathbf{b}_i from its ideal tetrahedral orientation and ψ_{ij} is the angle between \mathbf{b}_i and \mathbf{b}_j (see Fig. 3(a)). In this expression the direct

hydrogen bond energy, $\tilde{u}_{\alpha}(\phi)$, is described separately for donor and acceptor bonds, as denoted by the subscript α , and has the functional form of the data plotted in Fig. 3(c). Similarly, the effects of three-body interactions are described by $\tilde{v}_{\alpha\gamma}(\psi)$, which depends on the directionality of the bonds involved in ψ , denoted by α and γ , and has the functional form of the data in Fig. 3(d). The three-body effects are attenuated by $\lambda_{\alpha\gamma}$ based on the availability of broken hydrogen bond at a_i or a_j . The implementation of this three-body fluctuation model is described in complete detail in Supplemental Material [32].

The three-body fluctuation model exhibits interface-specific non-ideal hydrogen bond structure that is similar to that observed in atomistic simulation. As the inset of Fig. 4(a) illustrates, this includes an interfacial enhancement of donor-donor and acceptor-acceptor angles of $\psi < 60$ deg similar to that observed in atomistic simulation. We find that including the effects of three-body hydrogen bond defects significantly improve the ability of the model to accurately describe interfacial polarization and polarizability as illustrated in Fig. 2. These effects do not, however, completely account for the interfacial variations in $\langle (\delta \mu_{\bf \hat{n}}(a))^2 \rangle$, which suggests that interfacial polarizability likely contain additional contributions from other microscopic effects, such as higher-order many-body effects.

This mean-field model of interfacial hydrogen bonding has revealed two fundamental details about the molecular structure of the liquid water-vapor interface. First, the rigid tetrahedral model has revealed that the primary source of orientational constraints reflect the response of individual molecules to the anisotropic environment. Second, the three-body fluctuation model has revealed that this source of orientational constraints does not affect the polarization and polarizability. Rather, these dielectric properties vary at the interface due to collective molecular interactions, specifically in the form of three-body squeezed triangular hydrogen bond defects. These defects are especially common at the interface and structurally different from those that have been found to play an important role in orientational relaxation dynamics within the bulk liquid [40]. Here we have identified the origin of their enhanced interfacial stability and shown that their presence is consistent with a simple model of interfacial hydrogen bonding. This general theoretical framework for computing the orientational molecular structure of liquid water can be easily extended to systems with different interfacial environments, such as hydrated surfaces or non-aqueous molecular liquids.

We thank David Chandler, Liang Shi, and Rick C. Remsing for the useful discussions. This work was supported by the National Science Foundation under CHE-1654415 and also partially (SS) by the Kwanjeong Educational Foundation in Korea.

- * awillard@mit.edu
- [1] J. G. Kirkwood, J. Chem. Phys. 7, 911 (1939).
- [2] H. Fröhlich, Theory of dielectrics: dielectric constant and dielectric loss (Clarendon Press, 1958).
- [3] P. A. Bopp, A. A. Kornyshev, and G. Sutmann, Phys. Rev. Lett. 76, 1280 (1996).
- [4] F. Despa, A. Fernández, and R. S. Berry, Phys. Rev. Lett. 93, 228104 (2004).
- [5] D. J. Bonthuis, S. Gekle, and R. R. Netz, Phys. Rev. Lett. 107, 1 (2011).
- [6] R. Vácha, O. Marsalek, A. P. Willard, D. J. Bonthuis, R. R. Netz, and P. Jungwirth, J. Phys. Chem. Lett. 3, 107 (2012).
- [7] A. Schlaich, E. W. Knapp, and R. R. Netz, Phys. Rev. Lett. 117, 1 (2016).
- [8] R. J. Saykally, Nat. Chem. 5, 82 (2013).
- [9] P. Jungwirth and D. J. Tobias, Chem. Rev. 106, 1259 (2006).
- [10] Y. Levin, A. P. Dos Santos, and A. Diehl, Phys. Rev. Lett. 103, 1 (2009).
- [11] L. Zhao and Z. Lin, Soft Matter 7, 10520 (2011).
- [12] I.-F. W. Kuo and C. J. Mundy, Science **303**, 658 (2004).
- [13] C. D. Daub, D. Bratko, T. Ali, and A. Luzar, Phys. Rev. Lett. 103, 1 (2009).
- [14] N. Ji, V. Ostroverkhov, C. S. Tian, and Y. R. Shen, Phys. Rev. Lett. 100, 096102 (2008).
- [15] Y. R. Shen and V. Ostroverkhov, Chem. Rev. 106, 1140 (2006).
- [16] E. A. Raymond, T. L. Tarbuck, and G. L. Richmond, J. Phys. Chem. B 106, 2817 (2002).
- [17] E. A. Raymond, T. L. Tarbuck, M. G. Brown, and G. L. Richmond, J. Phys. Chem. B 107, 546 (2003).
- [18] M. A. Wilson, A. Pohorille, and L. R. Pratt, J. Phys. Chem. 91, 4873 (1987).
- [19] M. Matsumoto and Y. Kataoka, J. Chem. Phys 881 (1988).
- [20] Y. Fan, X. Chen, L. Yang, P. Cremer, and Y. Q. Gao, J. Phys. Chem. B 113, 11672 (2009).
- [21] A. P. Willard and D. Chandler, J. Phys. Chem. B 114, 1954 (2010).
- [22] P. A. Pieniazek, C. J. Tainter, and J. L. Skinner, J. Am. Chem. Soc. 133, 10360 (2011).
- [23] S. Nihonyanagi, T. Ishiyama, T. Lee, S. Yamaguchi, M. Bonn, A. Morita, and T. Tahara, J. Am. Chem. Soc. 133, 16875 (2011).
- [24] J. Kessler, H. Elgabarty, T. Spura, K. Karhan, P. Partovi-Azar, A. A. Hassanali, and T. D. Kuhne, J. Phys. Chem. B (2015).
- [25] A. E. Ismail, G. S. Grest, and M. J. Stevens, J. Chem. Phys. 125 (2006).
- [26] F. Sedlmeier, D. Horinek, and R. R. Netz, Phys. Rev. Lett. 103, 1 (2009).
- [27] F. P. Buff, R. A. Lovett, and F. H. Stillinger, Phys. Rev. Lett. 15, 621 (1965).
- [28] K. R. Mecke and S. Dietrich, Phys. Rev. E 59, 6766 (1999).
- [29] J. S. Rowlinson and B. Widom, *Molecular Theory of Capillarity* (Courier Corporation, 2002).
- [30] A. J. Patel, P. Varilly, S. N. Jamadagni, H. Acharya, S. Garde, and D. Chandler, Proc. Natl. Acad. Sci. U.S.A. 108, 17678 (2011).

- [31] A. P. Willard and D. Chandler, J. Chem. Phys. 141, 18C519 (2014).
- [32] See Supplemental Material at (URL will be inserted by publisher) for computational details.
- [33] M. W. Mahoney and W. L. Jorgensen, J. Chem. Phys. **112**, 8910 (2000).
- [34] S. J. Suresh and V. M. Naik, J. Chem. Phys. 113, 9727 (2000).
- [35] W. L. Jorgensen, J. Chandrasekhar, J. D. Madura, R. W. Impey, and M. L. Klein, J. Chem. Phys. 79, 926 (1983).
- [36] J. D. Smith, C. D. Cappa, K. R. Wilson, B. M. Messer, R. C. Cohen, and R. J. Saykally, Science **306**, 851 (2004).
- [37] J. D. Smith, C. D. Cappa, K. R. Wilson, R. C. Cohen, P. L. Geissler, and R. J. Saykally, Proc. Natl. Acad. Sci.

- U.S.A. **102**, 14171 (2005).
- [38] For the perfectly tetrahedral coordination, $\sum_{i=1}^{4} \mathbf{b}_i = 0$. Because of the symmetry, any pair of distinct i and j can represent the donor bonds such that $\langle \boldsymbol{\mu} \rangle = \mu_{\rm w} \langle \hat{\boldsymbol{\mu}} \rangle \propto \langle \mathbf{b}_i +$ $|\mathbf{b}_{j}\rangle = 0$ for any orientational distribution. The dipole vector also can be decomposed such that $\mu = \sum_{k=1}^{3} \mu_{\hat{\mathbf{e}}_k} \hat{\mathbf{e}}_k$ where $\hat{\mathbf{e}}_{k}$'s are orthonormal vectors in three dimensions. Choosing $\hat{\mathbf{e}}_1 = \hat{\mathbf{n}}$, we have $\langle \mu_{\hat{\mathbf{n}}} \rangle = \langle \mu \cdot \hat{\mathbf{n}} \rangle = \langle \mu \rangle \cdot \hat{\mathbf{n}} = 0$. Here $\boldsymbol{\hat{n}}$ could be other two unit vectors and there is no preference along specific direction. That is, since $|\mu|^2 = \sum_{k=1}^3 \mu_{\mathbf{\hat{e}_k}}^2 = \mu_{\mathbf{w}}^2$, we expect $\langle \mu_{\mathbf{\hat{n}}}^2 \rangle = \mu_{\mathbf{w}}^2/3$. [39] P. L. Geissler, Annu. Rev. Phys. Chem **64**, 317 (2013).
- [40] D. Laage and J. T. Hynes, Science **311**, 832 (2006).